AIAA JOURNAL
Vol. 44, No. 10, October 2006

Experimental Study of Supersonic Inlet Buzz

Simon Trapier,* Philippe Duveau,† and Sébastien Deck†
ONERA, 92322 Chatillon Cedex, France

DOI: 10.2514/1.20451

An experimental study of supersonic inlet buzz is presented. This study was carried out on a mixed compression rectangular inlet model; tests were done at Mach numbers ranging from 1.8 to 3, with and without bleed. Inlet flows were analyzed thanks to Schlieren videos and signal processing of unsteady pressure recordings. Two kinds of buzz were observed: "little buzz," which is thought to correspond to an acoustic resonance phenomenon excited by the presence of a shear layer under the cowl lip (*Ferri criterion*), and "big buzz," which seems to be triggered by a boundary layer separation on the compression ramps (*Dailey criterion*). In some cases, little buzz could be virtually suppressed by the introduction of a bleed. The frequency of big buzz is shown to be already present in the flow before the onset of large-amplitude oscillations, which suggests that the underlying mechanism of big buzz, probably linked to acoustics, already exists before buzz starts.

Nomenclature

A_c	=	inlet capture area, m^2
A_e	=	exit sonic throat area, m^2
A_∞	=	captured free streamtube area, m^2
c	=	speed of sound, m/s
f	=	frequency, Hz
M	=	Mach number
P_i	=	total pressure, Pa
P_{i0}	=	freestream total pressure, Pa
P_{RMS}	=	root mean squared pressure, Pa
PSD	=	power spectral density, Pa^2/Hz
Re	=	unit Reynolds number (dimensionless)
SPL	=	sound pressure level
T_0	=	stagnation temperature, K
ε	=	mass flow ratio, A_∞/A_c (dimensionless)
η	=	pressure recovery (dimensionless)

I. Introduction

INLET buzz is a phenomenon of self-sustained shock oscillations that may appear in almost every type of supersonic inlets, and which results in high-amplitude variations of the inlet mass flow and pressure. It generally arises when the entering mass flow is reduced below a given value. Inlet buzz can lead to thrust loss, engine surge, or even cause structural damages to the aircraft; this violent and dangerous phenomenon is therefore highly undesirable.

Inlet buzz was first observed and described by Oswatitsch [1] in 1944. Experimental, analytical and numerical studies have been carried out since, to get a better understanding of this phenomenon, and to avoid or delay its onset. Some progress has been made in the understanding of the physical mechanisms that trigger the instability. However, although several approximate methods have been proposed, it is today still impossible to precisely predict the onset of inlet buzz without several long and expensive wind tunnel experiments.

Our research aims at improving the quality of such a prediction. It is based upon experiments conducted in the ONERA supersonic wind tunnel S3MA, on a rectangular, mixed compression inlet model, for Mach numbers ranging from 1.8 to 3. This experimental setup is described as well as the test campaign and the first results are fully discussed in the present paper. Further analyses of the experimental data (using advanced signal processing methods) and numerical calculations of inlet buzz still are to be conducted and validated to estimate the ability of numerical methods to correctly simulate and predict this phenomenon.

II. Literature Review

After Oswatitsch's first observations, Ferri and Nucci [2], in 1951, and Dailey [3], in 1954, carried out the two main experimental studies on this topic, which allowed them to identify two different mechanisms that can trigger inlet buzz.

Ferri and Nucci observed that for axisymmetric external compression inlets operated in subcritical conditions, inlet buzz started when the shear layer issued from the intersection point of normal and oblique shocks entered the cowl lip and moved inside the inlet (this is known as the *Ferri criterion*). Indeed, the total pressure gradient across the shear layer, if strong enough, may lead to a flow separation below the cowl lip, which would choke the inlet front section and reduce the flow area, thus leading to the instability.

Dailey pointed out that the shock-induced flow separation on the external compression surface could have a similar effect. The boundary layer developing on the compression ramps separates when crossing the normal shock, and if the extent of this separated flow region increases, it may also cause an inlet obstruction and initiate buzz (*Dailey criterion*).

Dailey also noticed another important point: during buzz, the oscillation frequency depends on the diffuser length. The longer the diffuser is, the lower the frequency is. This fact suggests a link between the frequencies and the acoustic resonance modes of the diffuser.

Dailey compared the experimental frequencies with the acoustic modes of a closed-end organ pipe and found that the measured oscillation frequency is not associated with the fundamental mode, but with a higher harmonic one. The explanation of this fact is not clear; Dailey claims that the resonance frequency is influenced by vortex shedding from the cowl lip.

The role played by acoustic resonant modes in the frequency of shock oscillations in a diffuser was also shown by Sajben et al. [4,5].

Several other experimental studies of inlet buzz were carried out during the next years, on different inlet configurations, by Trimpi [6] in 1956, Fisher et al. [7] in 1970, and Nagashima et al. [8] in 1972.

Fisher et al. worked on a rectangular, external compression inlet. They observed two different instability phases, of similar frequencies but of different amplitude, called "little buzz" and "big buzz." When the mass flow through the inlet is reduced, little buzz suddenly appears, and further reduction of the mass flow initiates big buzz,

Received 10 October 2005; revision received 12 January 2006; accepted for publication 20 February 2006.

*Ph.D. Student, Applied Aerodynamics Department, 29 av. De la Division Leclerc.

†Research Scientist, Applied Aerodynamics Department, 29 av. De la Division Leclerc.

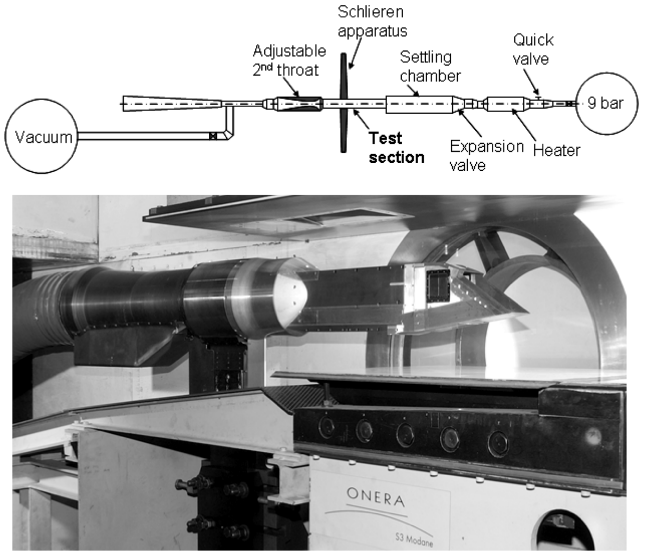

Fig. 1 Sketch of the wind tunnel and picture of the inlet model in the test section.

sometimes after an intermediate stable phase. Their experimental observations suggest that little buzz is triggered by a shear layer moving inside the cowl lip (Ferri criterion), whereas big buzz is associated with a separation of the ramp boundary layer (Dailey criterion).

Whereas these experiments allowed researchers to better understand the underlying physical mechanisms of inlet buzz, other authors got interested in the theoretical aspects of the problem. As soon as in 1951, Sterbentz and Evvard [9] submitted a linear analysis of the phenomenon: they consider the inlet as a Helmholtz resonator. Their main result is that the inlet should become instable if the slope of the pressure recovery characteristic is positive. Other theoretical studies about this subject were carried out, in particular by Trimpi [6] and Leynaert [10,11], but these kinds of linear analyses, based on highly idealized models and fluid flows, fail to give a precise representation of this complex phenomenon.

Few authors have so far tried to study inlet buzz numerically. To the authors' knowledge, Newsome [12] conducted the first unsteady Navier–Stokes computations of this phenomenon. Buzz flow appears only for a closed-end case, and the calculated frequency, 127 Hz, is very close to the theoretical fundamental acoustic mode (128 Hz), whereas the experimental result, 391 Hz, is associated with the third mode. In 1998, Lu and Jain [13] attempted to perform a numerical simulation of Dailey's experiments, using RANS equations and Baldwin–Lomax turbulence model. The inlet buzz flow seems to be well reproduced. The calculated frequency, around 28 Hz, agrees well with the experimental value of 25 Hz.

Table 1 Unit Reynolds number and stagnation temperature for the used Mach numbers

Mach number	Unit Reynolds number	Stagnation temperature
1.8	29×10^6	293 K
2	27×10^6	320 K
3	18×10^6	315 K

III. Experimental Setup

A. Wind Tunnel

The experiments were performed in the ONERA S3MA supersonic wind tunnel, located in Modane-Avrieux (Savoie, France). It is a blowdown wind tunnel, with a rectangular test section (0.80×0.76 m) and Mach numbers ranging from 0.1 to 5.5. Its maximum unit Reynolds number is 54×10^6; the possible running time is from 10 s to 15 min according to conditions (10–30 s with exhaust in vacuum storage tanks, 1–15 min with exhaust in atmosphere). Figure 1 shows a sketch of the wind tunnel, and the inlet model positioned in the test section.

Table 1 sums up the unit Reynolds numbers and stagnation temperatures corresponding to the used Mach numbers 1.8, 2, and 3.

B. Model

A drawing of the inlet model is given in Fig. 2. It is a rectangular, mixed compression supersonic inlet (approximately 85% external and 15% internal compression). The shock-on-lip Mach number, i.e., the Mach number where the ramp shocks hit the lip, is 2. The external compression is achieved by three ramps inclined by 5.5, 11.18, and 17.11 deg to the freestream flow direction. The internal surface of the cowl lip is inclined by 11.25 deg to the freestream flow direction. The

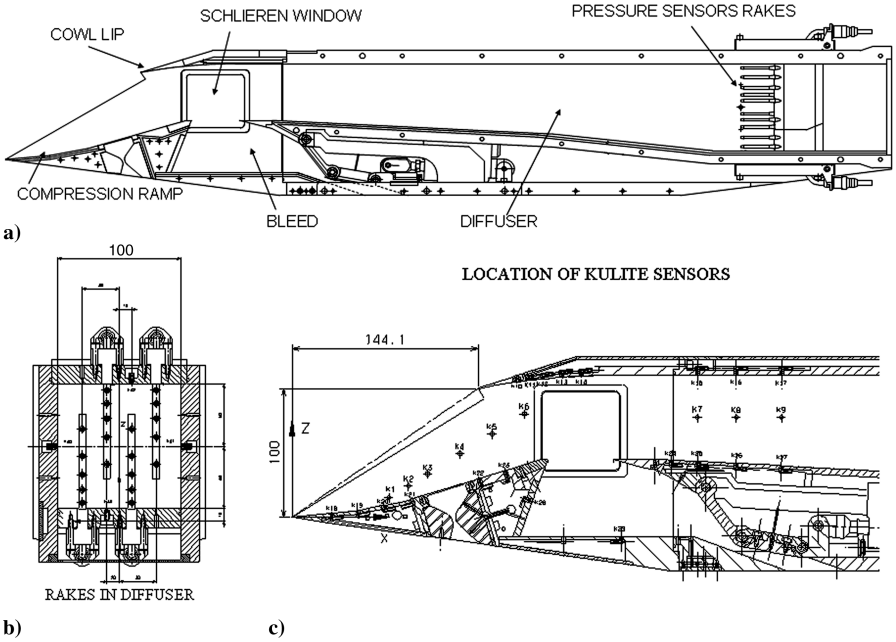

Fig. 2 Inlet model and its instrumentation.

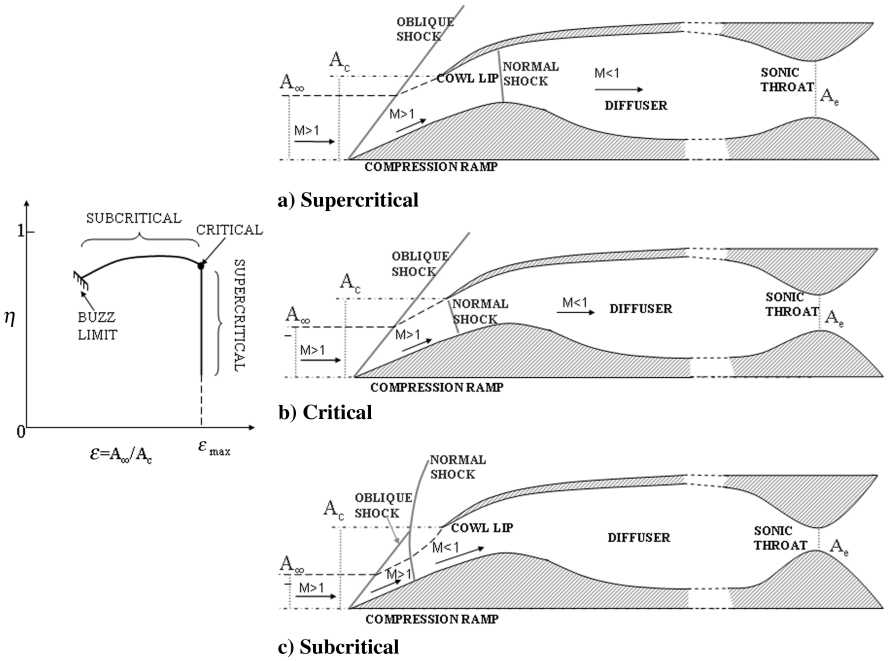

Fig. 3 Inlet characteristic and operations.

vertical height of the cowl lip above the ramp tip is 100 mm, and the inlet width is constant equal to 100 mm. The inlet capture area is $A_c = 0.01$ m^2.

The diffuser length is 535 mm. Its upper wall is horizontal, whereas its lower wall, initially horizontal, is inclined by 3 deg, then by 6.7 deg, so that the duct is divergent. The diffuser final section is square (100 × 100 mm).

The mass flow is measured by a sonic throat mass flow meter. This inlet can be throttled by a butterfly-type valve located between the diffuser end and the mass flow meter. The total length of the duct, between the cowl lip and the throttle, is 1861 mm.

The model is adaptable, and the inlet can be studied with or without bleed, or even with a perforated wall. The bleed, when existing, has an exit sonic section, the area of which is 10% of the inlet capture area.

Windows in the sidewalls allowed us to see, with Schlieren pictures and videos (500 frames/s), the flow and the shocks inside the inlet.

C. Location of Sensors

The model is equipped with a lot of pressure sensors. On the upstream part of the model, 30 Kulite sensors measured the unsteady static pressures on the compression ramp, on one sidewall, under the cowl lip, and inside the bleed chamber as shown in Fig. 2c. In the diffuser, four rakes with five total pressure sensors each, six static pressure sensors, and two Kulites allow us to estimate the pressure recovery of the inlet (Fig. 2b). The mass flow was measured by a sonic throat mass flow meter.

D. Test Procedure

Each inlet model configuration (with bleed or not, perforated wall, etc.) was tested for different Mach numbers ranging from 1.8 to 3. During every test, the exit throat, initially open, was progressively throttled to reduce the mass flow, until buzz started. Then the throat was opened back until buzz stopped.

Two kinds of measurements were carried out during these tests: either the steady values of pressure were recorded during the whole

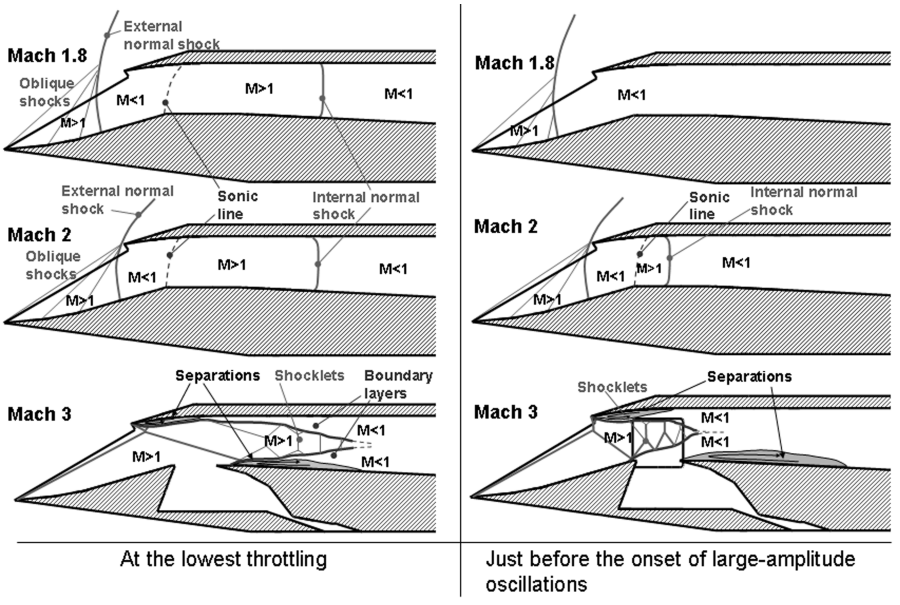

Fig. 4 Flow situation prior to buzz.

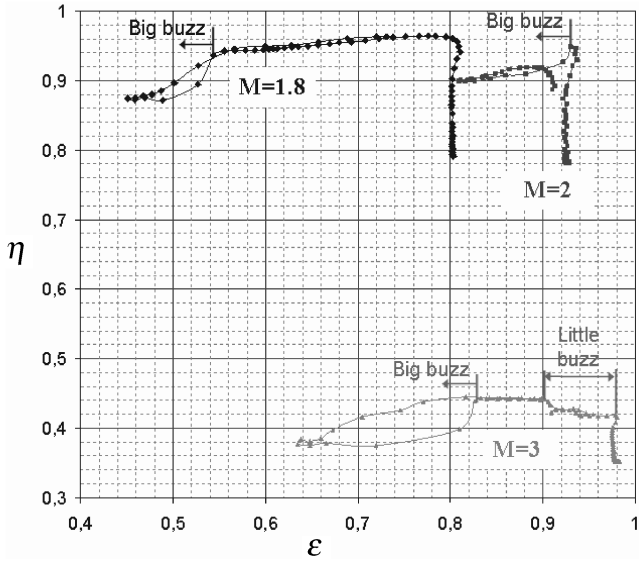

Fig. 5 Characteristic curves at three different Mach numbers with bleed.

duration of the test, or the unsteady values were recorded, with an acquisition frequency of 10 kHz, during 4–10 s, just when buzz has started. The first kind of measurements allowed us to plot the characteristic curves of the inlet; the second one made possible signal processing analyses, which can give us important information about the flow dynamics before and during the buzz.

IV. Initial Flow Pattern

This paragraph will firstly remind the different operating regimes of an external compression inlet and the corresponding flow patterns. Then the flow pattern prevailing at the beginning of the experimental measurements, at low throttling and before the onset of any instability, is described for Mach numbers 1.8, 2, and 3.

A. Inlet Operating Regimes

Let us remember that the characteristic curve of an inlet plots the pressure recovery against the mass flow coefficient. η is defined as the ratio of the mean total pressure at the end of the inlet duct to the freestream total pressure, and ε is the ratio of the area A_∞ of the free streamtube captured by the inlet to the capture area A_c. A_c represents the captured streamtube area in case of no spillage at 0 deg angle of attack.

$$\varepsilon = \frac{A_\infty}{A_c} \tag{1}$$

The characteristic curve usually has the appearance shown in Fig. 3. It features one vertical (constant ε) and one roughly horizontal branch (constant η). They correspond to different operation modes of the inlet which depend on the throttling, i.e. the downstream throat area A_e. At high A_e (Fig. 3a), the mass flow through the inlet is maximum ($\varepsilon = \varepsilon_{\max}$). The operating point lies on the vertical branch of the characteristic (supercritical operation). In this idealized inlet with one single ramp, there are two shocks: a first oblique shock, produced by the compression surface, and a normal shock that makes the flow subsonic, inside the inlet. For smaller A_e (Fig. 3b), the pressure inside the diffuser increases, and the normal shock moves upstream, until it is just attached to the cowl lip. The inlet is in critical operation. Reducing further A_e (Fig. 3c), the normal shock is expelled upstream of the cowl lip, on the compression ramp. The mass flow entering the inlet decreases; the operating point moves along the horizontal branch of the characteristic (subcritical operation). When the mass flow is even further reduced, the so-called buzz limit may be reached (left end of the horizontal branch). On the experimental curves that will be seen in Fig. 5 and 6, the loops on the left of the horizontal branches correspond to buzz cycles.

B. Initial Experimental Flow Pattern at Mach 1.8

Mach 1.8 is below the shock-on-lip Mach number. At low throttling, the inlet model operates supercritically. As explained in the preceding paragraph, there is at this regime an internal normal shock in the diffuser. However, our model is a mixed compression inlet in which the supercritical flow is not exactly like the idealized one of the external compression inlet shown previously (Fig. 3); in fact, there still remains an external normal shock due to the internal compression (Fig. 4, left). Note also that three oblique shocks intersect the external normal shock instead of one in the case of Fig. 3 because the external compression is achieved by three ramps.

At the beginning of the unsteady pressure recordings, just before the onset of large-amplitude oscillations, the flow is subcritical; the internal shock has been expelled, and only the external shock remains. The flow inside the inlet is fully subsonic (Fig. 4, right).

C. Initial Experimental Flow Pattern at Mach 2

The situation at Mach 2 is quite similar to the one at Mach 1.8. The shock-on-lip Mach number is 2, so the three oblique shocks are supposed to intersect right on the cowl lip. However, there still exists an external normal shock just upstream of the cowl lip like at Mach 1.8. The entering flow accelerates downstream of the cowl lip and is finally turned from supersonic to subsonic through a normal shock located in the diffuser. At low throttling, the internal shock is in the diffuser (Fig. 4, left). Just before the onset of large-amplitude oscillations, it has moved up to the location of the bleed chamber (Fig. 4, right) and the flow is almost critical.

D. Initial Flow Pattern at Mach 3

The flow is more complex. The oblique shocks issued from the ramps impact on the cowl internal profile, leading to a flow separation. The separated flow area generates an additional oblique

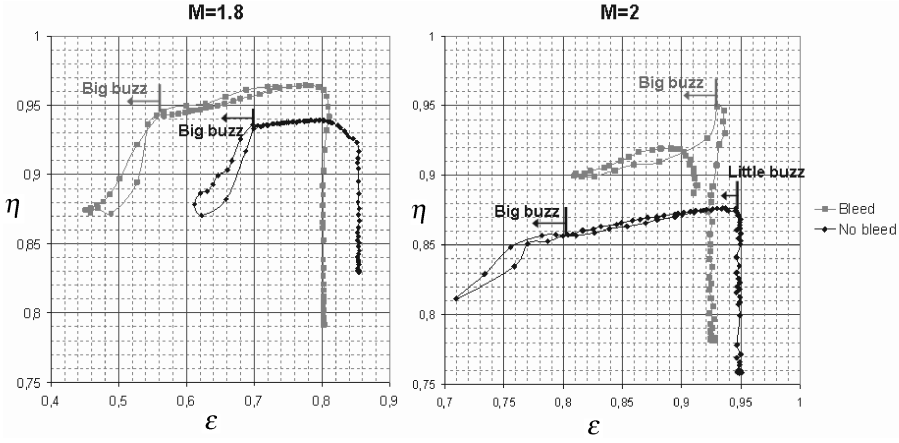

Fig. 6 Characteristic curves with or without bleed.

shock which impinges on the lower wall of the diffuser, downstream of the bleed chamber, thus creating a second separation. The supercritical flow regime is characterized by a diffuser flow pattern such as described by Sajben et al. [4] with several shocklets instead of a single normal shock. At low throttling these shocklets are in the diffuser (Fig. 4, left), and just before the onset of large-amplitude oscillations they are located above the bleed chamber (Fig. 4, right).

Note that, at the first two cases (Mach 1.8 and Mach 2), the initial supercritical flow patterns are similar whether there is bleed or not. At Mach 3, no test was conducted without bleed; that is why only the case with bleed is represented in Fig. 4.

V. Results and Discussion

The experimental results are discussed for Mach numbers 1.8, 2, and 3; the bleed effect is in particular studied. These flow conditions are selected because they cover all types of buzz initiation: from supercritical regime to critical and subcritical ones. In each case, steady pressure measurements and recordings are firstly used to get the characteristic curves, and then unsteady pressure signals are processed to identify the frequency response of the inlet before and during the cyclic oscillations. Schlieren visualizations are also helpful for the physical understanding of the phenomena.

The analysis of steady state measurements is presented in the first section, before focusing on the unsteady records in the second section.

A. Steady Measurements

In this paragraph a discussion of the influence of Mach number and bleed on the inlet performance is conducted, based upon the characteristic curves.

1. *Influence of Mach Number*

Figure 5 shows the characteristic curves of the inlet, at the three studied Mach numbers, for the test cases with bleed.

As expected, the curves greatly differ from one M number to another; the captured mass flow gets higher with increasing Mach number while pressure recovery is decreasing. The flow features are also fundamentally different as well as stability margins, as will be discussed in the second section.

2. *Influence of Bleed*

Figure 6 shows the characteristic curves of the inlet, plotted with and without bleed, at $M = 1.8$ and $M = 2$ (no test was conducted at $M = 3$ without bleed).

One can notice the major improvement in pressure recovery achieved thanks to the bleed device, but at the expense of a reduction of the captured mass flow. A consequence of this last point is that the buzz limit is shifted to a lower mass flow value for $M = 1.8$.

B. Unsteady Measurements

1. *Mach 1.8*

a. Before Buzz. At this Mach number, the buzz starts while the inlet is in subcritical operation, as described in Fig. 4. Figure 7 shows the spectra of two pressure signals recorded before buzz for the model without bleed. They represent the power spectral density (PSD) of the signal, i.e., the distribution in frequency of the mean squared value of the pressure. They are obtained with the Burg method (or maximum Entropy method) [14]. The ability of this autoregressive method to provide spectrum estimators with accurately resolved peaks (for both the frequency resolution and the energy level) allows more flexibility than the classical periodogram (see [15,16] for the use of this method in the field of fluid mechanics). The signals were recorded by the sensors K1 and K2, both located on the sidewall above the compression ramps (see their locations on the figure).

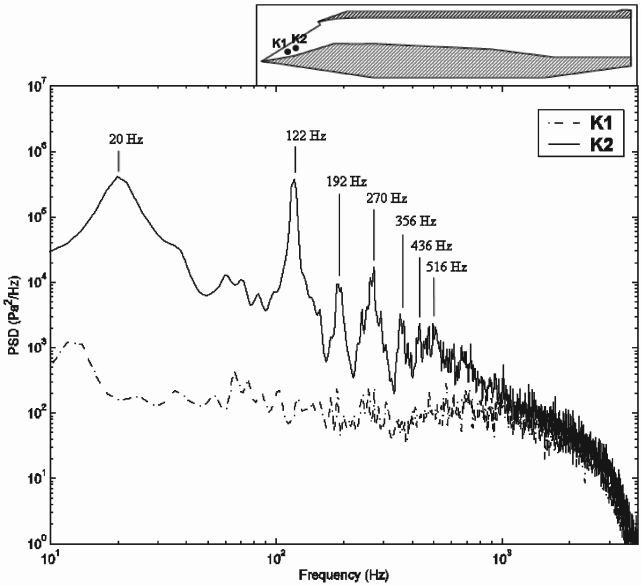

Fig. 7 Spectra of pressure signals prior to buzz ($M = 1.8$, no bleed).

The spectra of the unsteady pressure signals before buzz are of two types, depending on the sensor location. The sensors located upstream of the normal shock are in a supersonic flow region; they do not receive any information from the downstream part of the inlet. The spectrum has a broadband aspect characteristic of the turbulent fluctuation in the boundary layer; there is no particular frequency present in the signal (K1 in Fig. 7). Conversely, the spectra of the signals delivered by the sensors located downstream of the normal shock show several important peaks (K2 in Fig. 7). It is due to the fact that the normal shock is positioned between K1 and K2 before buzz onset.

We can observe the following on this spectrum:

1) A first important peak at 20 Hz, roughly corresponding to the buzz frequency which has still not occurred. This fact will be discussed hereafter.

2) A series of peaks of decreasing amplitude, the first and most important one at 122 Hz. These peaks may be attributed to the acoustic resonance modes of the inlet.

The resonance modes for a duct with an open and a closed end are given by the following formula [12]:

$$f_n = (2n + 1)\frac{c}{4L}(1 - M^2) \qquad n = 0, 1, 2 \ldots \tag{2}$$

where L is the length of the duct, c the speed of sound, and M the Mach number of the flow along the duct. According to our experimental data, the mean values between the subsonic diffuser and the flow choking section are $M = 0,35$ and $c = 344$ m/s. If one takes for L the distance between the cowl lip (open end) and the exit sonic throat acting acoustically like a closed end, one obtains $L = 1.861$ m.

The frequencies are gathered in Table 2.

These calculated frequencies agree well with the experimental peaks for $n \geq 1$, so we can conclude that these peaks correspond to the acoustic resonance modes of the inlet. The fundamental frequency $f_0 = 41$ Hz does not appear on the spectra; the reasons for that remain unclear, but similar phenomena have, however, been observed by other authors, in an axisymmetric supersonic inlet [3],

Table 2 Calculated and observed acoustic frequencies ($M = 1.8$, before buzz)

n	0	1	2	3	4	5	6
Calculated f_n	41 Hz	122 Hz	203 Hz	284 Hz	365 Hz	446 Hz	527 Hz
Observed peaks	——	122 Hz	192 Hz	270 Hz	356 Hz	436 Hz	516 Hz

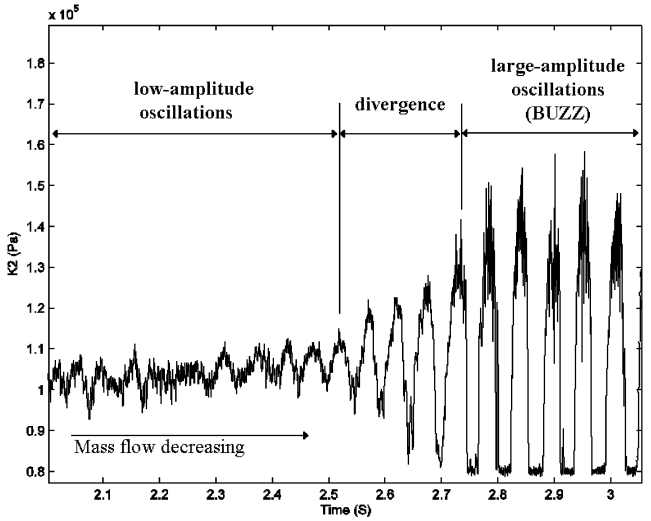

Fig. 8 Pressure signal K2 at buzz onset ($M = 1.8$, no bleed).

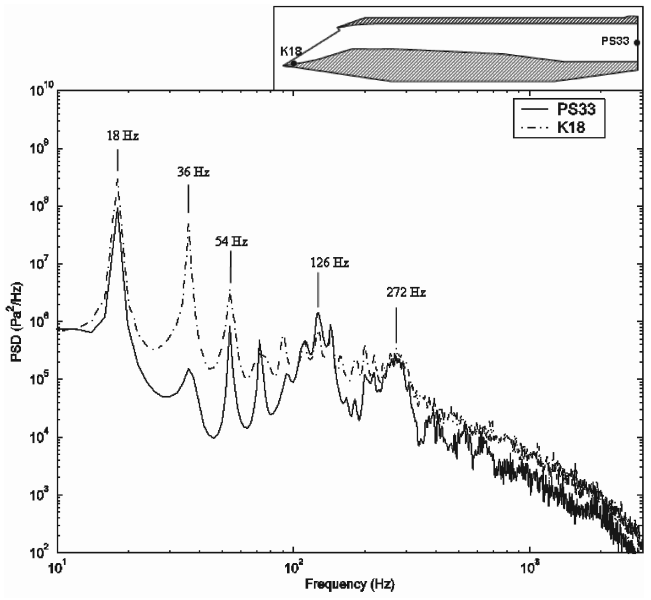

Fig. 9 Spectra of pressure signals during buzz ($M = 1.8$, no bleed).

or in a resonance tube with its open end in the face of a supersonic flow [17].

Concerning the 20 Hz oscillations, the Schlieren videos show that they are correlated with a motion of the normal shock, with a maximum amplitude of about 4.5 mm. These low-amplitude oscillations are taking place almost at the same frequency as those corresponding to large scale buzz. They seem to be amplified through a diverging process leading to the large oscillations of the buzz itself (Fig. 8).

This suggests that the physical mechanism at the origin of buzz is already present before the very beginning of the buzz, and is responsible for the smaller oscillations of the normal shock at the same frequency. The fact that the frequency is the same, whereas the amplitude of the shock displacement is very different, indicates that this frequency is very likely to be linked to an acoustic phenomenon (acoustic waves moving back and forth in the duct).

Bleed has almost no effect on the frequencies and amplitudes observed.

b. During Buzz. Figure 9 shows the spectra of the pressure signals recorded by sensors PS33 and K18 during buzz for the model with no bleed. PS33 is located in the diffuser end, and K18 is the most upstream sensor, located on the first compression ramp.

Although these two sensors are located far from each other, the frequencies appearing on the spectra of their signals are almost

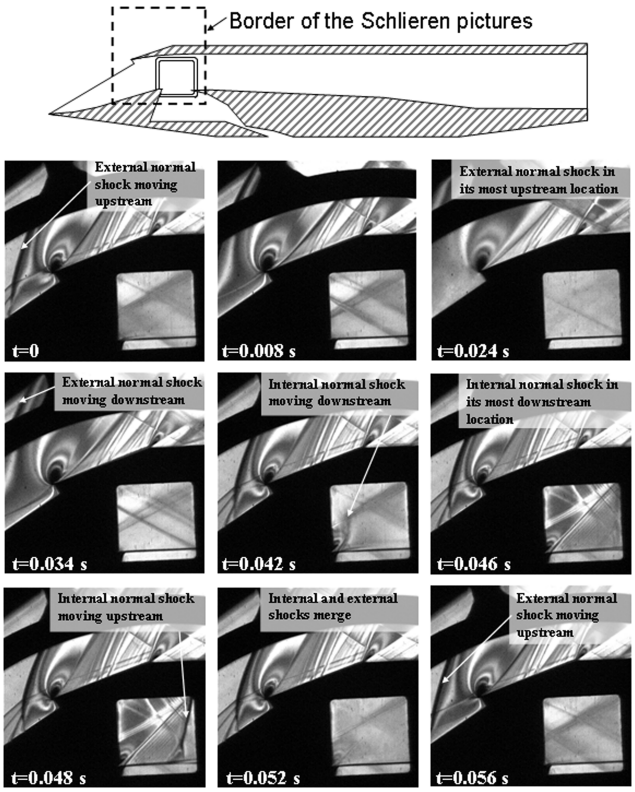

Fig. 10 Schlieren visualization of a buzz cycle ($M = 1.8$, no bleed).

identical. Indeed, the whole inlet is concerned by the very large-scale shock motion during buzz.

The main peak of these spectra corresponds to the buzz frequency at 18 Hz. The next peaks, at 36 and 54 Hz, are just harmonics of this fundamental frequency. Two other peaks of lower amplitude are noteworthy: the first one around 126 Hz and the second around 272 Hz. They are due to a secondary oscillation that takes place during a part of the buzz cycle, as we will see next.

Figure 10 shows nine Schlieren pictures taken during a buzz cycle. The part of the inlet that appears on the pictures is indicated at the top of the figure; it contains the cowl lip and the window in the sidewall. On the first two pictures, which were taken at $t = 0$ and 0.008 s ($t = 0$ is the beginning of the buzz cycle), the external shock is visible and is moving upstream. At $t = 0.024$ s it reaches its most upstream location. At $t = 0.042$ s, the external shock has moved back downstream, and an internal shock has entered the inlet (it is visible in the window). At $t = 0.046$ and 0.048 s the external shock is motionless and the internal shock moves back and forth inside the duct (the three oblique shocks issued from the external compression ramp are clearly evidenced on these latter pictures as well as the different shear layers). Then it merges with the external shock, which then moves upstream.

In Fig. 11 are plotted the pressure records of sensors K18 (ramp), K14 (cowl lip), and PS33 (diffuser end) during a buzz cycle. These plots show that there are three successive phases during a buzz cycle: a first phase during which the flow is subcritical (only the most upstream sensor K18 is located in a supersonic flow), a second one during which the external shock is expelled up to the ramp tip (the whole inlet flow is subsonic) and the secondary oscillations aforementioned occur, and a last phase during which a part of the internal flow becomes supersonic (K14, which is located inside the inlet, is in a supersonic flow).

The flow patterns during a buzz cycle are described in Fig. 12. During the first phase of the cycle, the flow is subcritical (Fig. 12a). The external normal shock is expelled upstream, almost up to the ramp tip; the separated zone on the compression surface grows up, and obstructs a significant part of the inlet section (Fig. 12b). The secondary oscillations around 126 and 272 Hz occur during this phase. Because of the obstruction, the entering mass flow decreases,

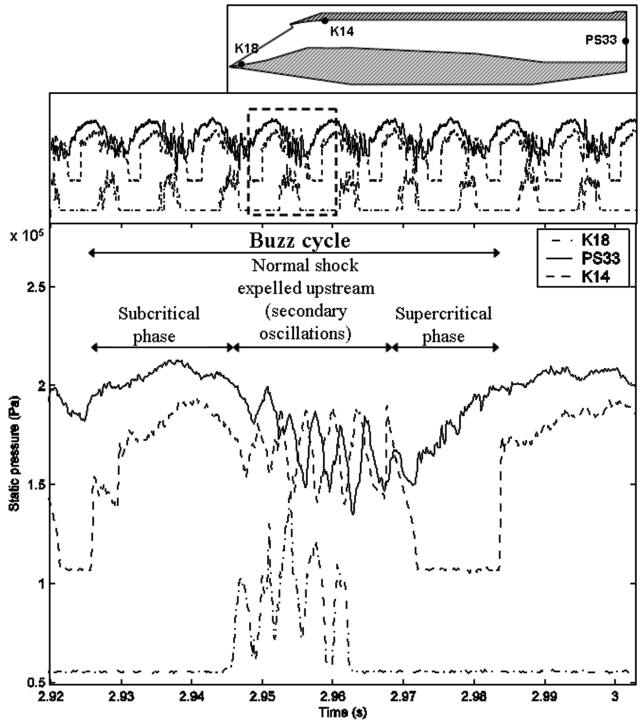

Fig. 11 Pressure signals during a buzz cycle ($M = 1.8$, no bleed).

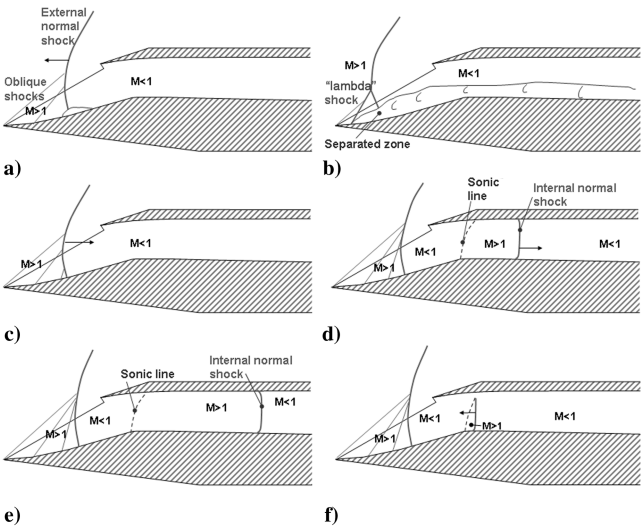

Fig. 12 Shock motion during a buzz cycle ($M = 1.8$, no bleed).

and the pressure inside the inlet consequently decreases (the mass flow measured by the sonic throat mass flow meter is in compliance with this description); when the pressure downstream of the shock is sufficiently low, the shock-induced separated flow area on the ramp disappears (Fig. 12c). The normal shock then bluntly moves downstream; an internal normal shock appears (Fig. 12d). The flow becomes like in supercritical conditions although the inlet throttling remains of subcritical nature (Fig. 12e). The inlet entrance is not obstructed anymore; the entering mass flow increases, and so does the pressure inside the inlet. The internal shock travels back upstream, and vanishes when arriving up to the subsonic region (Fig. 12f). The flow becomes subcritical again; the external shock is expelled because of the high pressure inside the inlet, and a new cycle may begin.

All these shock movements and pressure variations are guided by pressure acoustic waves going back and forth in the diffuser, which give a rhythm to buzz and force it to a regular frequency.

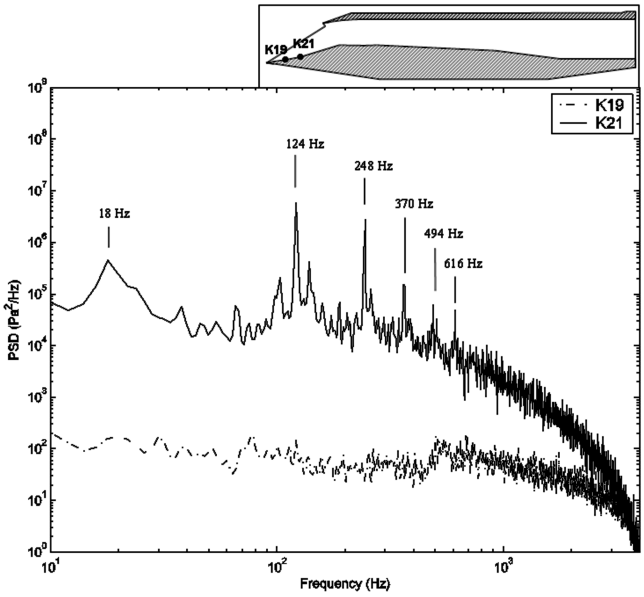

Fig. 13 Spectra of pressure signals prior to low-frequency buzz ($M = 2$, no bleed).

When a bleed device is introduced, a small frequency shift is observed (19 Hz instead of 18 Hz with no bleed). There is no major change in the amplitude, only a slight increase in high frequencies, probably because of the noise due to the bleed.

c. State of the Boundary Layer. The boundary layer over a flat plate is known to become turbulent when the Reynolds number reaches approximately 2 million at Mach 1.8 and 2, and 1.5 million at Mach 3. In our case, according to the unit Reynolds numbers of the flow (see Table 1), this would mean that the transition takes place around 0.07 m downstream of the ramp tip, i.e., in the middle of the second ramp. Upstream of this point, the boundary layer is laminar, and is therefore more likely to separate. This could trigger the blunt growth of the separated flow area, when the normal shock reaches this point. However, the localization of the boundary layer transition using the Reynolds number is very imprecise, and we have no reliable experimental way to determine whether the boundary layer is turbulent or not, so this can only remain a hypothesis.

2. *Mach 2*

At $M = 2$ there may exist two different types of oscillations which will be called "little buzz" and "big buzz." When it is present, the little buzz starts as soon as the regime is critical (see Fig. 6).

a. Little Buzz. The spectra of the signals recorded by sensors K19 and K21 (both located on the compression ramp) before the low-frequency buzz starts are plotted in Fig. 13.

Whereas the spectrum of K19 is flat (sensor located in a supersonic zone), the one of K21 shows an important peak at 124 Hz and its harmonics, but also a peak at 18 Hz.

The frequency of this latter peak is already the same as that of the lower frequency buzz beginning later. This was also observed at Mach 1.8 for probably the same physical reason. So was the case of the 124 Hz peak which corresponds to an acoustic mode of the internal duct; its amplitude is, however, much higher at Mach 2 than at Mach 1.8.

This amplitude is, in fact, roughly the same as the one of the low-frequency buzz, as we can see on the pressure recordings (Fig. 14). It can be considered as another kind of buzz. Like in Fisher et al. experiment [7], this new type of buzz that occurs as soon as the flow is subcritical will be called little buzz in the present paper, whereas the one which appears later will be called big buzz.

This little buzz is also linked with a back-and-forth motion of the shocks, with a lower amplitude than during big buzz. Schlieren pictures showing this motion can be seen in Fig. 15: the external normal shock moves upstream as far as the location of sensor K20 ($t = 0$ and 0.002 s), then it moves back downstream, and an internal

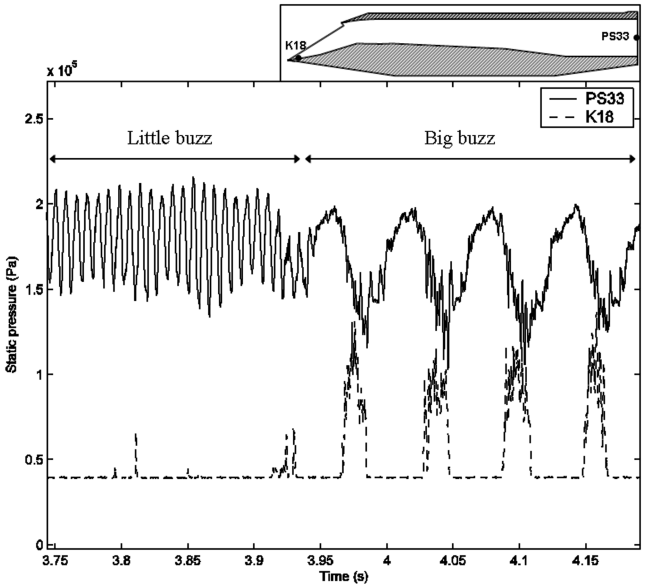

Fig. 14 Transition between little buzz and big buzz ($M = 2$, no bleed).

shock travels downstream to the location of sensor K14. This internal shock is visible on the picture taken at $t = 0.004$ s.

According to Fisher et al., little buzz is due to a shear layer entering the cowl lip (Ferri criterion); this shear layer is issued from the intersection of the external normal shock with one of the oblique shocks generated by the ramps. In the present case, there are three ramps generating three oblique shocks and consequently three shear layers. The upper one, issued from the intersection of the normal shock and the first oblique shock, is the strongest one in terms of total pressure difference across it. At $M = 1.8$, before the onset of big buzz, this upper shear layer does not enter the cowl lip. Only the two lower ones do. But at $M = 2$, the three of them are swallowed by the inlet, and in particular the strongest one, for the oblique shocks are more inclined (Fig. 16). This may explain that the amplitude of the little buzz is much higher at $M = 2$ than at $M = 1.8$.

The total pressure differences analytically determined across each shear layer are indicated in Fig. 16. According to Fisher et al., the minimum value of $\Delta P_i/P_{i0}$ for a shear layer passing under the cowl lip to trigger little buzz is 7%.

This observation tends to confirm the link between little buzz and shear layer ingestion by the inlet. It has been already noticed that the

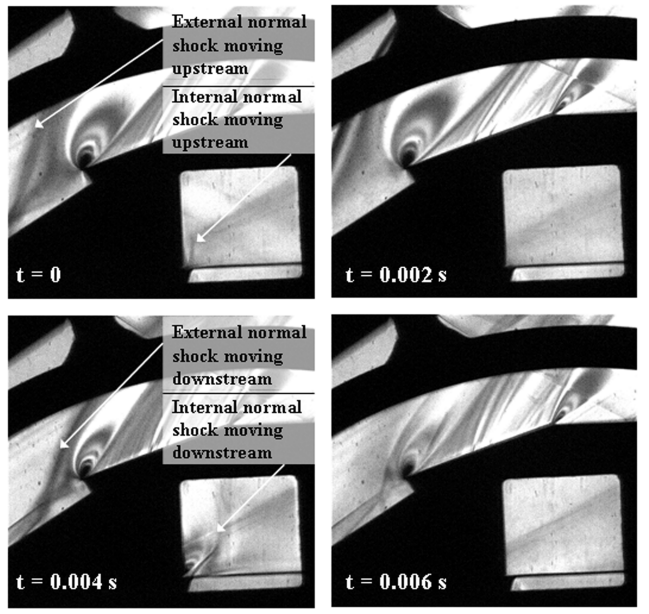

Fig. 15 Schlieren visualization of a little buzz cycle ($M = 2$, no bleed).

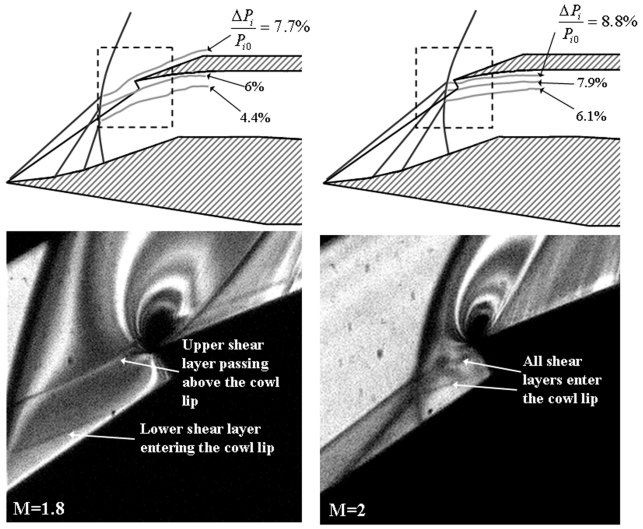

Fig. 16 Shear layers at $M = 1.8$ and $M = 2$.

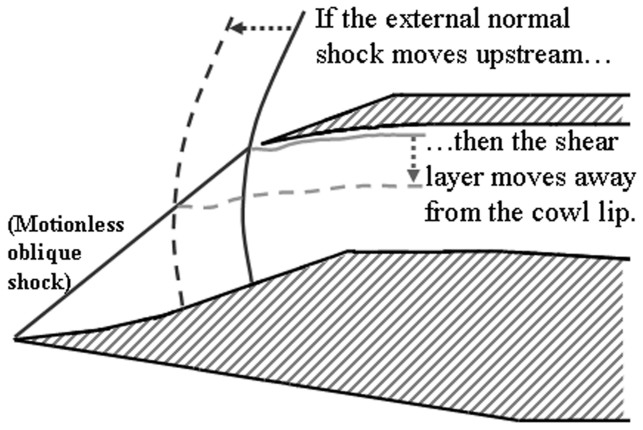

Fig. 17 Motion of the shear layer resulting of a shock motion.

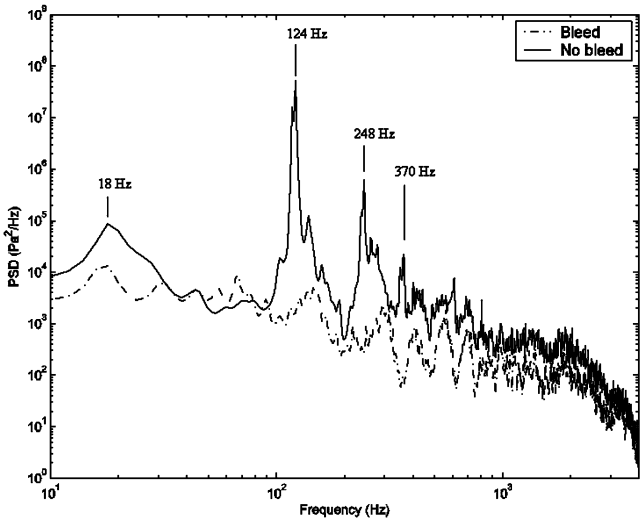

Fig. 18 Spectrum of little buzz oscillations, with and without bleed ($M = 2$).

frequency of the little buzz corresponds to a resonance mode of the duct. This suggests that the presence of a shear layer below the cowl lip can sustain or even amplify this acoustic resonance.

Our hypothesis to explain this fact is the following: if compression waves traveling from downstream (due to the reduction of the downstream sonic throat) reaches the normal shock, this shock is pushed upstream to match the back pressure conditions. As a consequence the normal shock intersects the oblique shocks more upstream than in the previous situation. Hence the intersection points and the resulting shear layers move away from the cowl lip and get closer to the compression ramps (Fig. 17).

This results in the ingestion by the inlet of more low total pressure flow above the shear layers leading to a decrease of the average total pressure level inside the inlet. This mechanism is much the same as if the compression waves had been reflected into expansion waves. Note that it is by the way what occurs at the open end of a duct.

If the total pressure difference across the shear layer is strong enough, the reflected waves will be of higher amplitude than the incident ones, and the resonance phenomenon will be amplified. This leads to a self-excited oscillation as described, for instance, in [18]. The feedback mechanism is the reflection of the pressure waves on the exit sonic throat.

Contrary to big buzz, little buzz is not triggered by sudden variations of the mass flow. Indeed, there is no indication, neither on Schlieren pictures nor in pressure records, suggesting the existence of a separated flow under the cowl lip which could obstruct the inlet section and reduce the entering mass flow. The only effect of the shear layers passing beneath the cowl lip is the total pressure variation. The physical mechanisms at the origin of little buzz and big buzz are therefore fundamentally different, which could explain that they do not occur at the same frequencies.

b. Influence of Bleed. The spectra of the pressure signals recorded by sensor PS33 during tests with and without bleed are plotted in Fig. 18.

Bleed virtually eliminates the little buzz. Indeed, bleed stabilizes the internal normal shock, which almost stands still above the bleed chamber instead of oscillating. Bleed absorbs pressure waves and the resonance is damped.

c. Big Buzz. The transition from little buzz to big buzz is almost instantaneous (Fig. 14). The low-frequency oscillations (18 Hz) are very similar to those that take place at $M = 1.8$ and they probably have the same physical causes: a shock-induced separation on the ramp boundary layer. Indeed, just before the big buzz starts, the Schlieren pictures show the upper part of a "lambda" shock, characteristic of a shock-induced separation (Fig. 19). The oblique shock visible on this figure cannot be one of those generated by the compression ramps because its slope is too high; indeed, the shock-on-lip Mach number is 2. This shock must therefore be due to a flow separation.

The pressure records also show that the normal shock passes upstream of sensor K18, i.e., on the first compression ramp, for the first time just before the onset of big buzz (see Fig. 14). The flow in this area has only crossed one oblique shock, so the normal shock gets stronger. This could explain why the separated flow area suddenly extends at this time and triggers big buzz.

d. Influence of Bleed. The effects of bleed on big buzz can be seen in Fig. 20. They are more pronounced at $M = 2$ than at $M = 1.8$.

1) The amplitude of the oscillations is reduced by the presence of the bleed ($P_{\mathrm{RMS}}/P_{i0} = 3.8\%$, instead of 12%, at the end of the diffuser).

2) The frequency is slightly increased (from 19 to 20 Hz).

3. *Mach 3 (With Bleed)*

This case is more complex than the preceding ones because of the supercritical flow regime prevailing before the buzz onset. Schlieren pictures are also not as helpful as previously for physical understanding due to a lack of contrast.

With regard to the frequencies, not only two types of pressure signals (before big buzz and during big buzz) are obtained as the exit throat is throttled, but at least four. In this case it is worthwhile to study the change in time of the spectral structure of data. Figure 21 compares the spectrograms of the signal recorded by PS33 (end of diffuser) at $M = 1.8$, $M = 2$, and $M = 3$: the spectrogram is a three-dimensional plot which shows how the energy of the process is decomposed over time and frequency.

At $M = 3$, four successive phases are visible on the spectrogram:

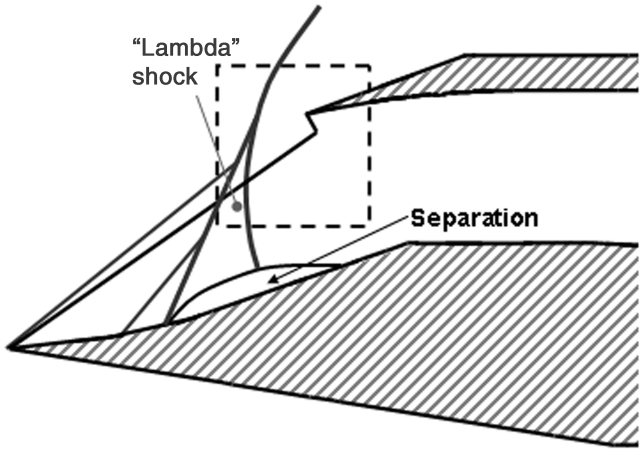

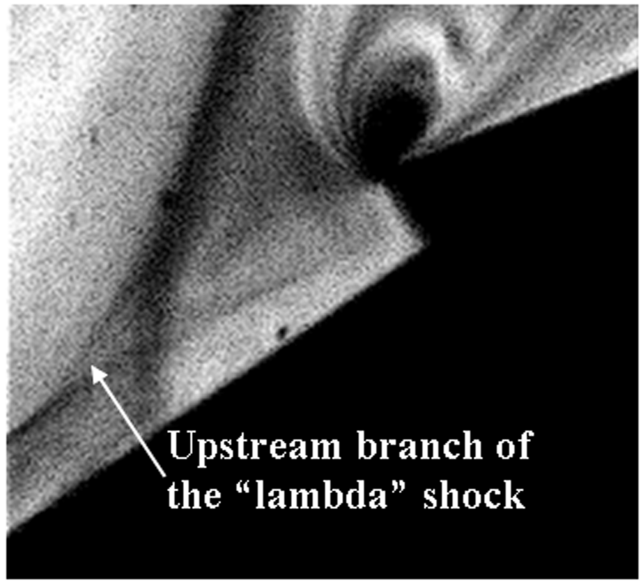

Fig. 19 Lambda shock showing the presence of a separation on the ramp ($M = 2$).

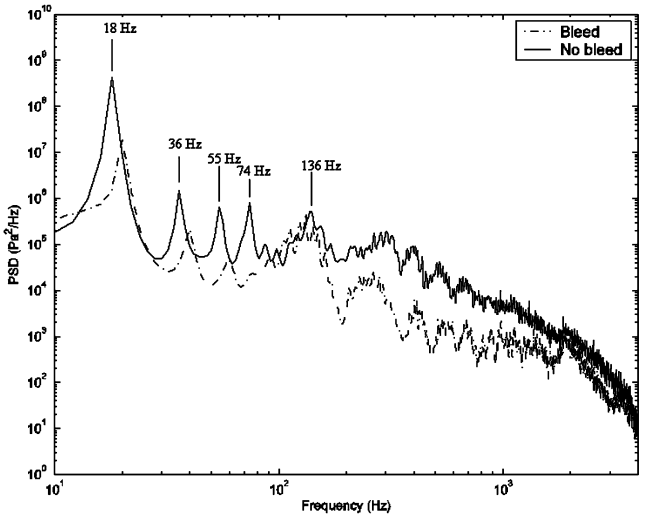

Fig. 20 Spectra of big buzz oscillations, with and without bleed ($M = 2$).

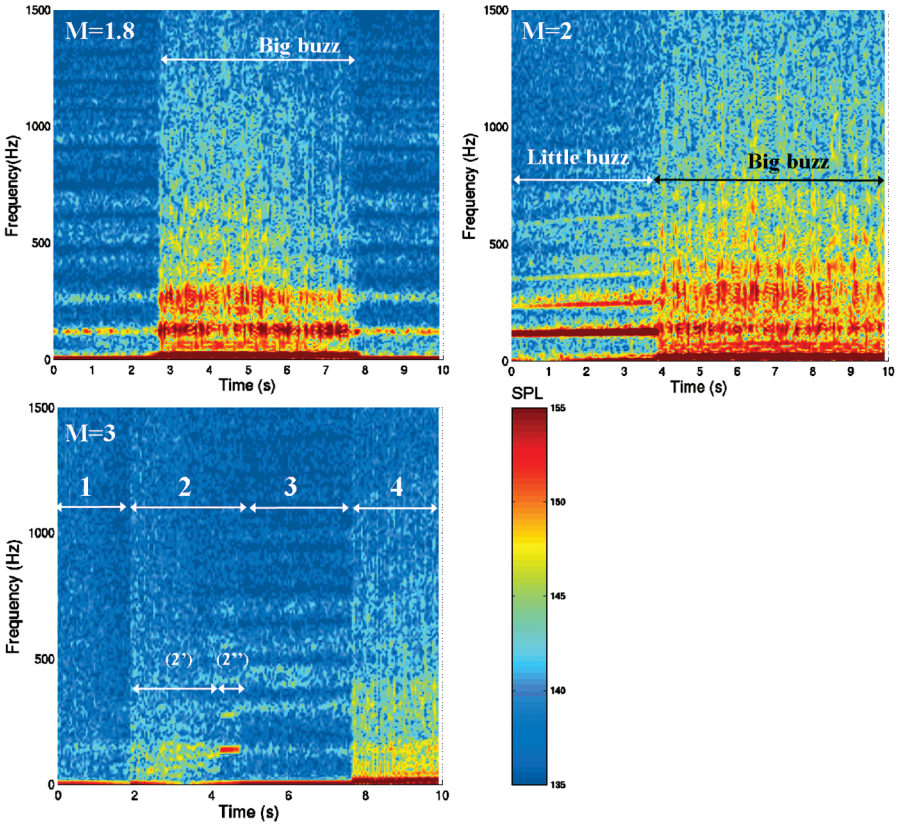

Fig. 21 Spectograms of pressure signal PS33 at $M = 1.8$, $M = 2$ and $M = 3$.

Phase 1: There are almost no pressure fluctuations, except those in the turbulent boundary layer ($P_{\mathrm{RMS}}/P_{i0} = 0.76\%$).

Phase 2: Larger oscillations appear ($P_{\mathrm{RMS}}/P_{i0} = 1.6\%$). They are quite irregular in a first step (phase 2′) then their frequency gets stabilized around 138 Hz (phase 2″). This latter phase looks similar to the little buzz observed in the preceding cases.

Phase 3: The oscillations are damped ($P_{\mathrm{RMS}}/P_{i0} = 0.79\%$) but the same frequencies still seem to be present.

Phase 4: Big buzz appears ($P_{\mathrm{RMS}}/P_{i0} = 8.2\%$). Its frequency is 12 Hz.

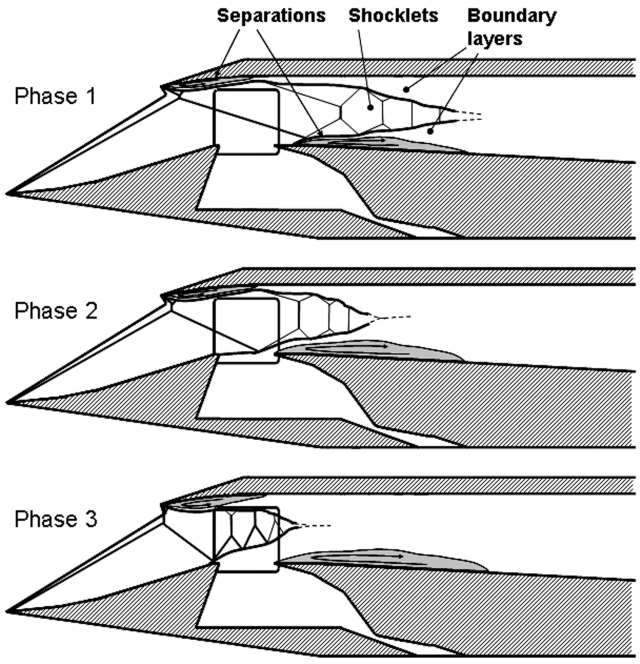

Fig. 22 Flow patterns prior to big buzz at Mach 3.

As the Schlieren pictures do not allow us to directly see the flow pattern inside the inlet, we can only make assumptions about it. These assumptions are based on the pressure recordings, and on analogies with the observations at lower Mach numbers. The flow patterns are represented in Fig. 22.

During phase 1, the flow is supercritical, such as described in the preceding section.

When the exit section is throttled, the pressure inside the diffuser grows up and the Mach number decreases. The oblique shock issued from the cowl lip gets steeper and steeper, and the whole system of shocklets moves upstream until the separated flow area located on the lower wall reaches the downstream edge of the bleed. At this moment, the pressure sensors located in the bleed receive for the first time information from the downstream flow. The oscillations of little buzz start: phase 2 begins. The fact that the oscillations can start only

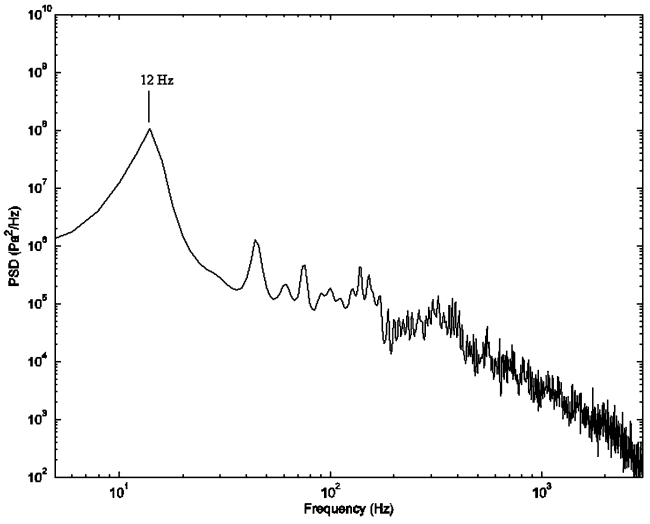

Fig. 23 Spectrum of big buzz oscillations in the diffuser end ($M = 3$).

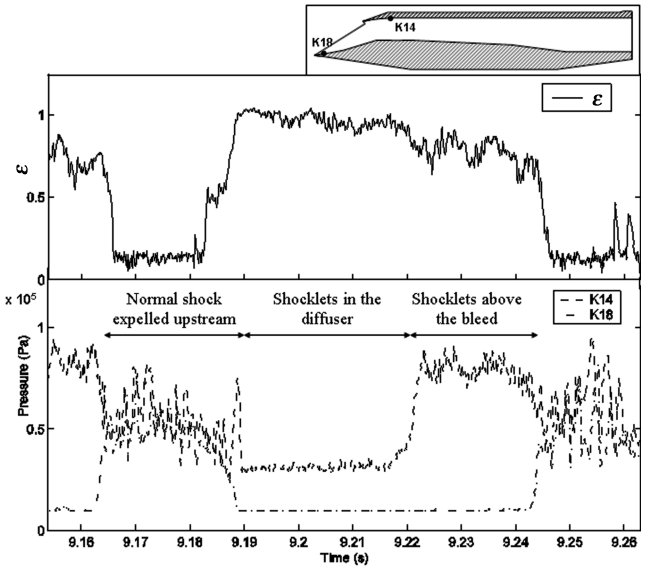

Fig. 24 Mass flow ratio and pressure signals during a big buzz cycle ($M = 3$).

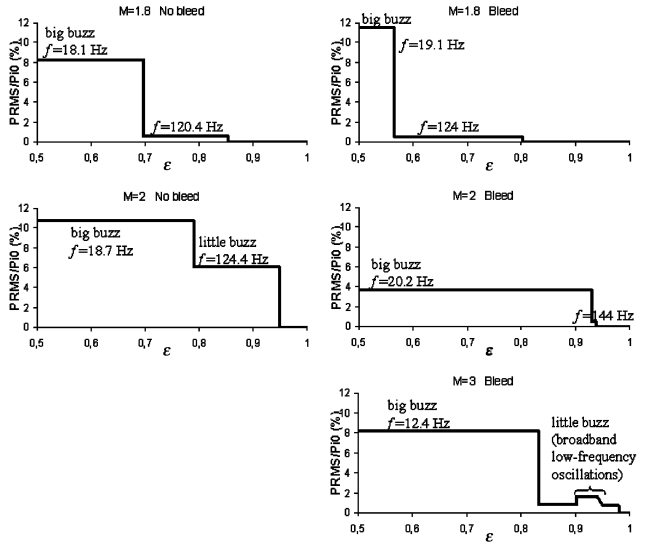

Fig. 25 Flow oscillations as a function of entering mass flow.

once the separated area has reached the bleed is not explained, nor is the origin of their frequency. The flow inside the duct is totally inhomogeneous which makes simple acoustic analysis impossible.

When the shocklets move further upstream, they stand above the bleed and get stabilized, as already seen at $M = 2$. The oscillations of little buzz are damped (phase 3).

Finally, approximately when the shocklets reach the upstream edge of the bleed, a large separation appears on the compression surface. The internal shocks are expelled upstream and big buzz starts.

The spectrum of the signal of PS33 (diffuser end) during big buzz is shown in Fig. 23. The mass flow ratio ε and the pressure recorded by K18 (ramp) and K14 (cowl lip, above the bleed) during a big buzz cycle are plotted in Fig. 24.

At the beginning of the cycle, a large separated flow area on the compression surface obstructs the inlet. The external normal shock is expelled upstream and the mass flow is low. The high-frequency secondary oscillations that were already observed at lower Mach numbers are still present.

Because of the low entering mass flow, the internal pressure falls until the flow separation on the ramps disappears. The external shock then moves downstream and shocklets appear in the diffuser. The flow pattern is of supercritical nature again and similar to the one that was prevailing before big buzz during phase 1 (Fig. 22). The mass flow increases together with the internal pressure, so the shocklets are pushed upstream above the bleed where they stabilize (like during phase 3, cf. Fig. 22). The entering mass flow remains high, the internal pressure keeps growing, and the shocks are finally expelled upstream. The flow on the compression ramps separates and a new cycle begins.

No test was conducted at $M = 3$ without bleed, so we cannot evaluate its effect. But we can suppose that, like at $M = 2$, the bleed has a positive influence: it tends to reduce the boundary layer thickness and to stabilize the shocks.

VI. Conclusion

Figure 25 sums up the different phases encountered during the flow oscillations and presents the entering mass flow ratio at which they take place and their frequencies for the five different test cases. The oscillations are represented by the P_{RMS} of the pressure signal recorded at the end of the diffuser.

Two types of oscillations were observed: 1) the little buzz, which may occur as soon as the inlet operates subcritically and whose frequency was ranging from 120 to 140 Hz, and 2) the big buzz, arising at lower entering mass flows (higher throttling) and characterized by larger amplitudes and lower frequencies (around 20 Hz at $M = 1.8$ and $M = 2$, and 12.4 Hz at $M = 3$).

The flow patterns were described for each case, and hypotheses have been proposed about the physical mechanisms at the origin of the oscillations. Little buzz is thought to correspond to an acoustic resonance of the inlet excited by the presence of a shear layer under the cowl lip (Ferri criterion), whereas big buzz seems to be triggered by a separated flow area located on the compression surface which obstructs the inlet entrance (Dailey criterion). Little buzz is particularly intense at the shock-on-lip Mach number ($M = 2$) but can efficiently be damped by the introduction of bleed device.

It has, however, to be noticed that the buzz and its onset can dramatically change from one inlet configuration to another. The results obtained on this rectangular mixed compression inlet model should not therefore be directly generalized.

However, it has to be kept in mind that the experimental results presented in the present paper only are the first part of a larger research, and will now be used as a reference for further analyses and for numerical simulations.

Acknowledgments

The authors are grateful to J. M. Massonat (ONERA/CMA), who conducted the experiments herein described. P. Sagaut (LMM/Paris 6) is also acknowledged for his support to this thesis work.

References

[1] Oswatitsch, K., "Der Druckrückgewinn bei Geschossen mit Rückstossantrieb bei hohen Übershallgeschwindigkeiten (Der Wirkungsgrad vos Stossdiffusoren)," *Bericht Nr. 1005 Forsch. und Entwickl. des Heereswaffenamtes (Göttingen)*, 1944.

[2] Ferri, A., and Nucci, L. M., "The Origin of Aerodynamic Instability of Supersonic Inlets at Subcritical Conditions," NACA RM L50K30, 1951.

[3] Dailey, C. L., "Supersonic Diffuser Instability," Ph.D. Thesis, California Institute of Technology, Pasadena, CA, 1954.

[4] Bogar. T. J., Sajben, M., and Kroutil, J. C., "Characteristic Frequencies in Transonic Diffuser Flow Oscillations," *AIAA Journal*, Vol. 21, No. 9, 1983, pp 1232–1240.

[5] Sajben, M., Bogar. T. J., and Kroutil, J. C., "Experimental Study of Flows in a Two-Dimensional Inlet Model," AIAA Paper 83-0176, Jan. 1983.

[6] Trimpi, R., "A theory for Stability and Buzz Pulsation Amplitude in Ram Jets and an Experimental Investigation Including Scale Effects," NACA Report 1265, 1956.

[7] Fisher, S. A., Neale, M. C., and Brooks, A. J., "On the Sub-Critical Stability of Variable Ramp Intakes at Mach Numbers Around 2," National Gas Turbine Establishment Report No. ARC-R/M-3711, England, Feb. 1970.

[8] Nagashima, T., Obokata, T., and Asanuma, T., "Experiment of Supersonic Air Intake Buzz," Institute of Space and Aeronautical Science, Report No. 481 (Vol. 37, No. 7), Tokyo, Nov. 1972.
[9] Sterbentz, W., and Evvard, J., "Criterions for Prediction and Control of Ram-Jet Flow Pulsations," NACA RM E51C27, 1951.
[10] Leynaert, J., "Une Description Globale Élémentaire du Pompage des Prises d'Air Supersoniques," Note Technique ONERA 47/2149 A, 1968.
[11] Leynaert, J., "Pompage Dans les Entrées d'Air Supersoniques," *L'Aéronautique et l'Astronautique*, Vol. 6, No. 22, 1970, pp 47–62.
[12] Newsome, R. W., "Numerical Simulation of Near-Critical and Unsteady, Subcritical Inlet Flow," *AIAA Journal*, Vol 22, No 10, 1984, pp. 1375–1379.
[13] Lu, P. J., and Jain, L. T., "Numerical Investigaton of Inlet Buzz Flow," *Journal of Propulsion and Power*, Vol 14, No. 1, Jan.–Feb. 1998, pp. 90–100.
[14] Burg, J. P., "Maximum Entropy Spectral Analysis," *Modern Spectrum Analysis*, edited by D. G. Childers, IEEE, New York, 1978, pp. 34–41.
[15] Larchevêque, L., Sagaut, P., Lê, T. H., and Comte, P., "Large Eddy Simulation of a Compressible Flow in a Three-Dimensional Open Cavity at High Reynolds Number," *Journal of Fluid Mechanics*, Vol 516, Oct. 2004, pp 265–301.
[16] Deck, S., "Numerical Simulation of Transonic Buffet over a Supercritical Airfoil," *AIAA Journal*, Vol 43, No 7, pp 1556–1566, 2005.
[17] Brocher, E., and Duport, E., "Resonance Tubes in a Subsonic Flowfield," *AIAA Journal*, Vol 26, No 5, 1988, pp. 548–552.
[18] Hankey, W. L., and Shang, J. S., "Analysis of Self-Excited Oscillations in Fluid Flows," AIAA Paper 80-1346, 1980.

M. Auweter-Kurtz
Associate Editor